

# Selective Switching Between Two Band-Edge Alignments in Ternary Pentagonal CdSeTe Monolayer: Atom-Valley Locking

Zhi-Qiang Wen<sup>1</sup>, Qiu Yang<sup>1</sup>, Shu-Hao Cao<sup>1</sup>, Zhao-Yi Zeng<sup>2,\*</sup>, Hua-Yun Geng<sup>3</sup>, Xiang-Rong

Chen<sup>1,\*</sup>

<sup>1</sup> College of Physics, Institute of Atomic and Molecular Physics, Sichuan University,

Chengdu 610065, China;

<sup>2</sup> College of Physics and Electronic Engineering, Chongqing Normal University, Chongqing

401331, China;

<sup>3</sup> National Key Laboratory for Shock Wave and Detonation Physics Research, Institute of

Fluid Physics, CAEP, Mianyang 621900, China

## Abstract:

In the field of photocatalytic water splitting, no current studies have explicitly investigated the coexistence of multiple band-edge alignments in two-dimensional (2D) materials with intrinsic electric fields. In this Letter, we designed the ternary pentagonal CdSeTe monolayer, and proposed a novel concept called atom-valley locking, which could provide multiple band-edge positions. In the CdSeTe monolayer, two distinct valleys emerge in the electronic structure, one contributed by Se atoms and the other by Te atoms, with a spontaneous polarization of 187 meV between them. This phenomenon can be attributed to the localization of valley electrons and the breaking of four-fold rotational reflection symmetry, yet it does not rely on the breaking of time-reversal symmetry. Due to the atom-dependent valley distribution, two types of band-

---

\* Corresponding authors. E-mail: [zhaoyizeng@cqnu.edu.cn](mailto:zhaoyizeng@cqnu.edu.cn); [xrchen@scu.edu.cn](mailto:xrchen@scu.edu.cn)

edge alignments can be identified. Moreover, selective switching between them can be achieved by strain engineering, thereby enabling precise control over the site of the hydrogen evolution reaction. Our findings open up new opportunities for exploring valley polarization and provide unique insights into the photocatalytic applications of 2D materials with intrinsic electric fields.

**Keywords:** Atom-valley locking; Valley polarization; Band-edge alignment; Photocatalytic water splitting; CdSeTe monolayer

Valley, as an intrinsic degree of freedom for electrons, have become a hot topic in condensed matter physics in recent years [1-5]. It has been proven that the valley degree of freedom can couple with other electronic degrees of freedom, leading to various physical phenomena such as spin-valley coupling [5-12], valley-layer coupling [9,13-16], and valley-orbit coupling [17-19]. Especially, in spin-valley locked materials, applying a transverse electric field can generate spin-polarized currents via the valley Hall effect [3,20,21]; selectively exciting specific valley with circularly polarized light [22-26] can induce corresponding spin polarization; and manipulating valley polarization [27-31] allows for control over spin-dependent electron transport. These studies indicate that manipulating valleys through external means enables more efficient control of spin, offering extensive possibilities for the design of next-generation spintronic devices [32-41].

Could the manipulation of valleys enable the applications in other fields, such as the solar-driven hydrogen production from water splitting [42]? The answer is

affirmative. For a traditional photocatalyst, a bandgap larger than 1.23 eV is necessary to straddle the redox potential of water [43]. However, Li *et al.* [44] discovered that two-dimensional (2D) materials with intrinsic electric fields can break this limitation, enabling infrared-light-driven photocatalytic water splitting, which significantly improves the utilization of solar energy. Since then, many 2D materials with intrinsic electric fields [45-48] have been investigated, with band-edge alignment emerging as their most distinctive and significant feature. According to the spatial distribution of carriers in the valence-band maximum (VBM) and conduction-band minimum (CBM), four types of band-edge alignments [49,50] can be identified in these materials. When the VBM and CBM are contributed by atoms from a single surface, only one type of band-edge alignment is present. When the VBM or CBM involves contributions from both surfaces, multiple types of band-edge alignments can coexist [51-54]. However, current studies have focused on the dominant one, with limited discussion on the roles of the others.

In this Letter, we design a ternary pentagonal CdSeTe monolayer and propose a novel concept called atom-valley locking, which has two outstanding features: 1) unlike the layer-valley coupling [9,13-16,55,56], the valleys in the CdSeTe monolayer are confined within sublayers composed of only a single type of atom, making the valley distribution atom-dependent. 2) a spontaneous valley polarization of 187 meV is achieved without the typical requirement of breaking time-reversal symmetry [14], which is attributed to the localization of valley electrons and the breaking of four-fold rotational reflection symmetry. Owing to this unique distribution of valleys, two types

of band-edge alignments are present, and the selective switching between them can be achieved by modulating valley polarization through strain engineering, enabling precise control over the location of the hydrogen evolution reaction. These findings offer new possibilities for exploring valley polarization and provide unique insights into the photocatalytic applications of 2D materials with intrinsic electric fields.

Our calculations were performed using the Vienna *ab initio* Simulation Package (VASP) [57,58] with the exchange-correlation function of Perdew-Burke-Ernzerhof (PBE) [59]. The cutoff energy was set to 500 eV, and the convergence criteria of force and energy were set to  $10^{-7}$  eV/Å and  $10^{-10}$  eV, respectively. To prevent the interlayer interactions, a vacuum layer of 20 Å was selected along the *z*-direction, and the DFT-D4 method [60] was adopted to describe the weak van der Waals (vdW) interactions between adjacent layers. The phonon dispersion curve was obtained in a  $6 \times 6 \times 1$  supercell based on the finite differences approach. The *ab initio* molecular dynamics (AIMD) simulation was performed at 300 K for 10 ps with a time step of 2 fs in a  $4 \times 4 \times 1$  supercell.

In Figs. 1(a) and 1(b), we illustrate the optimized crystal structures of the ternary pentagonal CdSeTe monolayer and its binary counterpart, i.e. CdSe<sub>2</sub> monolayer. In Table I, we summarize the obtained structural parameters, including lattice constants, thickness, and bond lengths, as well as the independent elastic constants. We first examine the dynamic stability, thermal stability, and mechanical stability of the CdSeTe monolayer. In Fig. 1(c), the absence of imaginary frequencies in the phonon dispersion curve indicates its dynamic stability. Fig. 1(d) presents the AIMD simulation, where he

energy fluctuates within a narrow range, with no significant structural deformation or bond disruption, thereby confirming its thermal stability. The independent elastic constants meet the Born criteria ( $C_{11} > 0$ ,  $C_{66} > 0$ , and  $C_{11} > |C_{12}|$ ) [61], suggesting its mechanical stability.

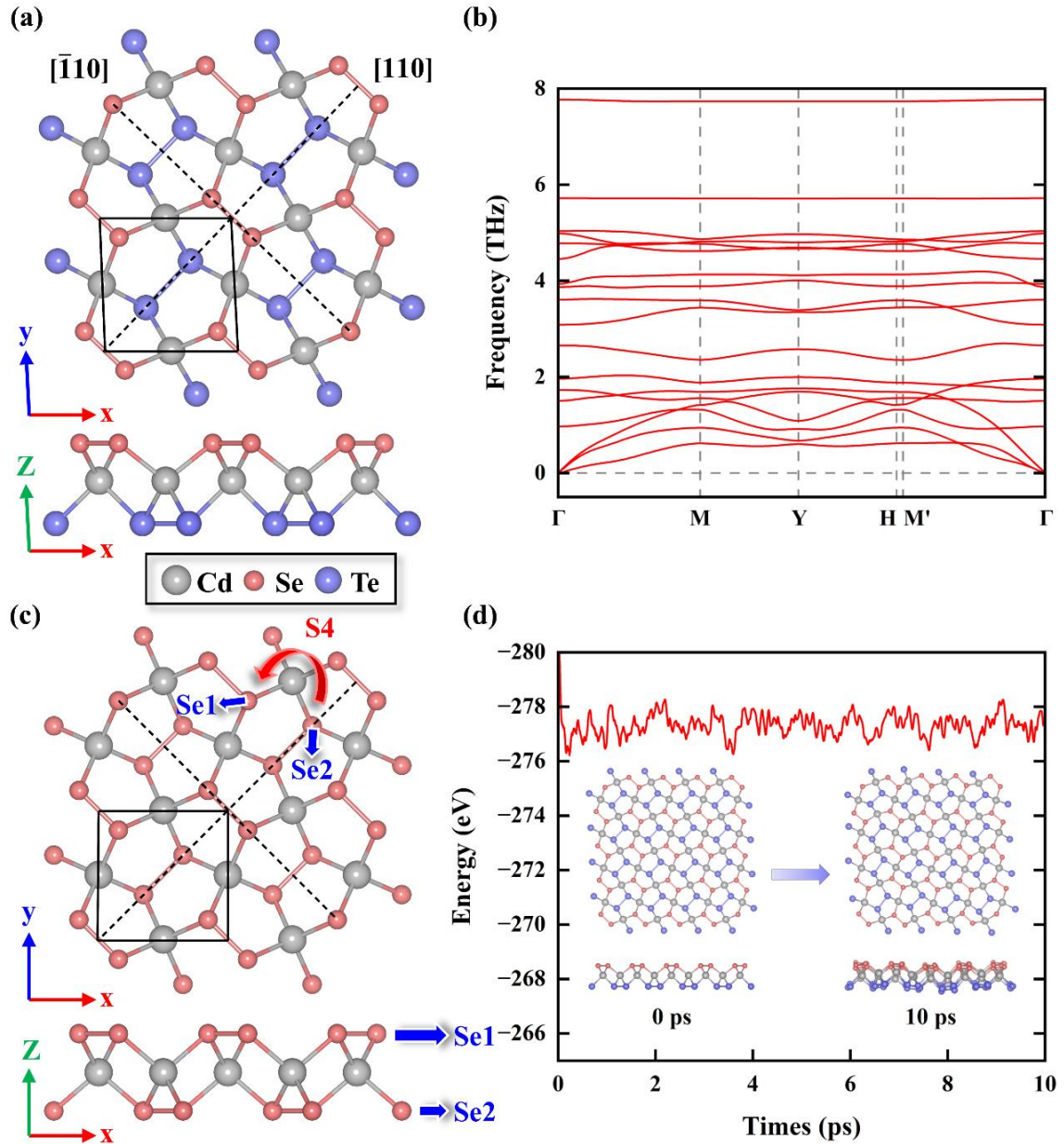


**FIG. 1** (Color online) The optimized crystal structures of (a) CdSeTe and (b) CdSe<sub>2</sub> monolayers. The black solid lines represent the unit cell, the black dashed lines indicate two perpendicular mirror symmetry planes, and the labels [110] and  $[\bar{1}10]$  denote the

directions of the applied in-plane uniaxial strains. The red arrow marks the four-fold rotational reflection axis through Cd atom, while the blue arrows highlight the two distinct groups of Se atoms. (c) The phonon dispersion curve and (d) AIMD simulation of the CdSeTe monolayer.

**TABLE I.** The obtained lattice constants  $a$  (Å), thicknesses  $h$  (Å), bond lengths ( $d_{\text{Cd-Se}}$ ,  $d_{\text{Cd-Te}}$ ,  $d_{\text{Se-Se}}$ , and  $d_{\text{Te-Te}}$ ) (Å), and the independent elastic constants ( $C_{11}$ ,  $C_{12}$ ,  $C_{22}$ , and  $C_{66}$ ) (N/m) of the CdSeTe and CdSe<sub>2</sub> monolayers.

Materials	$a$	$h$	$d_{\text{Cd-Se}}$	$d_{\text{Cd-Te}}$	$d_{\text{Se-Se}}$	$d_{\text{Te-Te}}$	$C_{11}$	$C_{12}$	$C_{22}$	$C_{66}$
CdSeTe	5.72	3.46	2.69	2.83	2.40	2.77	11.97	4.09	21.14	6.14
CdSe <sub>2</sub>	5.54	3.31	2.67	–	2.40	–	–	–	–	–

Now, we investigate how the atom-valley locking is achieved in the ternary pentagonal CdSeTe monolayer. To fully understand the origins of this phenomenon, it is necessary to include its binary counterpart in the subsequent discussion. The projected band structures of both monolayers at the HSE06 level [62] are shown in Figs. 2(a) and 2(b), with the former highlighting elemental contributions and the latter detailing atomic contributions. Both monolayers are semiconductors with indirect bandgaps of 1.45 eV for the CdSeTe monolayer and 2.27 eV for the CdSe<sub>2</sub> monolayer. We find that each monolayer exhibits two valleys in the conduction band, located along the high symmetry paths  $\Gamma$ – $M$  and  $\Gamma$ – $M'$ , respectively. However, notable differences can be observed between them. In the CdSe<sub>2</sub> monolayer, the two valleys are solely

contributed by Se atoms and exhibit energetic degeneracy. In contrast, the two valleys in the CdSeTe monolayer are contributed by Se and Te atoms, respectively, with a polarization of 187 meV between them. Unlike the valley-layer coupling observed in certain bilayers [9,13,15,16] and altermagnets [55,56], the valley distribution in the CdSeTe monolayer is atom-dependent. Both the valley and layer polarization arise spontaneously within the material, with no need for external assistance.

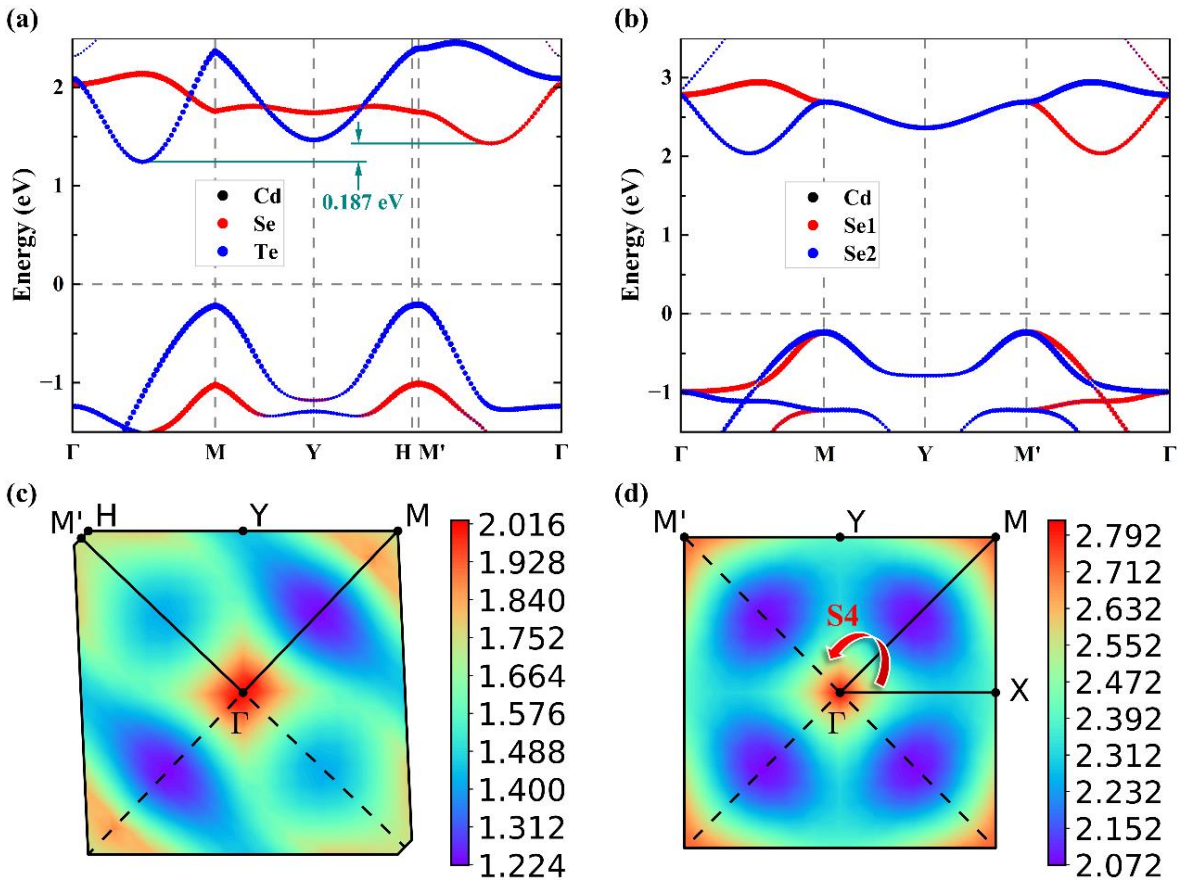


**FIG. 2** (Color online) The electronic band structures of (a) CdSeTe and (b) CdSe<sub>2</sub> monolayers at the HSE06 level. The CdSe<sub>2</sub> monolayer does not follow the conventional high symmetry path  $\Gamma$ - $X$ - $M$ - $\Gamma$  because the energetic degeneracy of the valleys does not signify their equivalence. The conduction-band edges of (c) CdSeTe and (d) CdSe<sub>2</sub> monolayers throughout the first Brillouin zones. The solid black lines represent the

irreducible Brillouin zones, while the dashed black lines and red arrow indicate their structural symmetries.

It is known that symmetry plays a crucial role in determining valley behavior, so it is essential to analyze the structural symmetries of both monolayers. The CdSe<sub>2</sub> monolayer has a square unit cell, two perpendicular mirror symmetry planes, and a four-fold rotational reflection (S<sub>4</sub>) axis through Cd atoms, belonging to the space group  $P\bar{4}2_1m$  (No. 113). It is noteworthy that the S<sub>4</sub> symmetry connects two different groups of atoms, Se<sub>1</sub> and Se<sub>2</sub>. The irreducible Brillouin zone (BZ) of the CdSe<sub>2</sub> monolayer is triangular ( $\Gamma-X-M-\Gamma$ ) [63], which transforms into a square first BZ through mirror reflections and S<sub>4</sub> operation, as shown in Fig. 2(d). However, the CdSeTe monolayer has a rhombic unit cell and two perpendicular mirror symmetry planes, belonging to the space group  $Cmm2$  (No. 35). It is important to note that while substituting Se<sub>2</sub> with Te breaks the S<sub>4</sub> symmetry, it does not lead to significant changes in the crystal structure. The irreducible BZ of the CdSeTe monolayer is trapezoidal ( $\Gamma-M-Y-H-M'-\Gamma$ ) [64], and only mirror reflections are required to transform it into a hexagonal first BZ, as shown in Fig. 2(c).

In the CdSe<sub>2</sub> monolayer, the S<sub>4</sub> symmetry connects the high symmetry paths  $\Gamma-M$  and  $\Gamma-M'$ , protecting the valleys along these paths and resulting in their energetic degeneracy. Furthermore, the spatial separation between two sublayers is about 3.31 Å, which is as large as the typical interlayer distance in multilayer van der Waals materials [65], leading to minimal hybridization of the electronic wavefunctions between them

[66]. As a result, electrons in these valleys are highly localized around Se1 and Se2 atoms, and their charge densities exhibit the S4 symmetry, as shown in Figs. 3(c) and 3(d). In contrast, the lack of the S4 symmetry in the CdSeTe monolayer leaves the valleys along these paths unprotected, resulting in their polarization. Additionally, the spatial separation between two sublayers is about 3.46 Å, causing the electrons in these valleys to be highly localized around Se and Te atoms. However, their charge densities no longer exhibit S4 symmetry, as shown in Figs. 3(a) and 3(b). In brief, the atom-valley locking and spontaneous valley polarization observed in the CdSeTe monolayer can be attributed to the localization of the valley electrons and the breaking of the S4 symmetry. Most importantly, the time-reversal symmetry remains intact due to the absence of magnetism and an external magnetic field, despite that breaking this symmetry is typically a prerequisite for valley polarization [14].

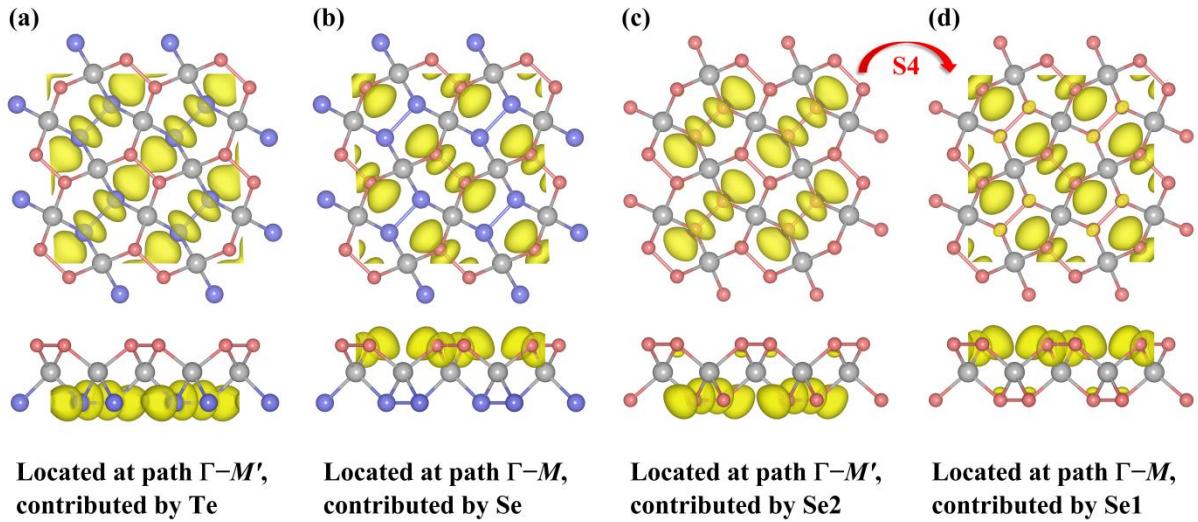


**FIG. 3** (Color online) The partial charge densities of the valleys in the CdSeTe monolayer (a,b) and CdSe<sub>2</sub> monolayer (c,d). The isosurface value is set to  $0.004 e/\text{\AA}^3$ . The red arrow indicates that the partial charge densities of the valleys in the CdSe<sub>2</sub> monolayer exhibit the S4 symmetry, while in the CdSeTe monolayer, they do not.

We then discuss the coexistence of two types of band-edge alignments in the CdSeTe monolayer. It is known that, to be a suitable photocatalyst for water splitting, a material must have an appropriate bandgap (1.23–3 eV) and band-edge positions that straddle the redox potential of water [43]. The absolute band-edge positions of each valley can be obtained from [49,67]:  $E_{\text{VB}}^{\text{abs}} = E_{\text{VB}}^{\text{DFT}} - V_{\text{VAC}}$ ,  $E_{\text{CB}}^{\text{abs}} = E_{\text{CB}}^{\text{DFT}} - V_{\text{VAC}}$ , where  $E_{\text{VB/CB}}^{\text{DFT}}$  denotes the energies of the valence-band or conduction-band valleys at the HSE06 level, and  $V_{\text{VAC}}$  represents the vacuum level. In 2D materials with intrinsic electric fields, each surface exhibits a different vacuum level. Therefore, which  $V_{\text{VAC}}$  should be subtracted in the above equations requires further discussion and remains a common challenge faced by these materials in photocatalytic applications. The band-edge alignment can be categorized into four types based on the spatial distribution of valley carriers. As illustrated in Figs. 4(a)–4(d), the valleys distributed on different surfaces exhibit distinct absolute band-edge positions. This not only affects the band-edge alignment but also causes the oxygen evolution reaction (OER) and hydrogen evolution reaction (HER) to occur on different surfaces of the material [45].

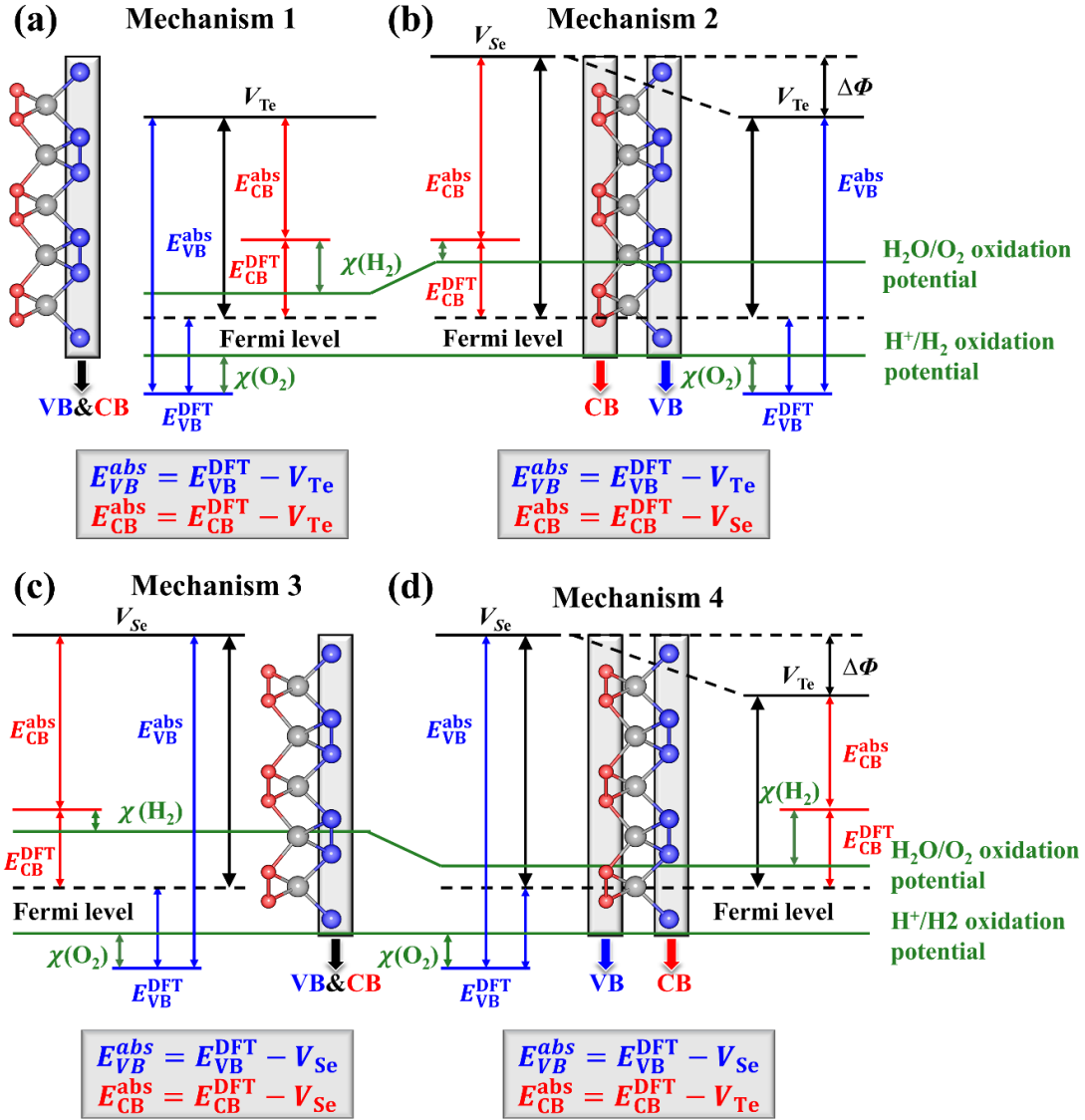


**FIG. 4** (Color online) (a)–(d) Four types of band-edge alignments. The blue, red and black arrows indicate the spatial distribution of the valence-band and conduction-band valleys. The green lines represent the redox potential of water, and the energy difference between this potential and the absolute band-edge positions of each valley determines the overpotential for the OER and HER ( $\chi(O_2)$  and  $\chi(H_2)$ ).

As a 2D material with an intrinsic electric field, a vacuum level difference ( $\Delta\Phi$ ) of 0.26 eV can be found between two surfaces of the CdSeTe monolayer. The valence-

band valleys are solely contributed by Te atoms, causing photogenerated holes to localize on the lower surface, while the conduction-band valleys, due to the unique atom-valley locking, are contributed by both Se and Te atoms, resulting in photogenerated electrons being distributed on both surfaces. As a result, the CdSeTe monolayer exhibits two types of band-edge alignment simultaneously, corresponding to Alignment 1 and Alignment 2 shown in Figs. 4(a) and 4(b). When Alignment 1 is active, the HER occurs on the lower surface; when Alignment 2 is active, the HER occurs on the upper surface. The absolute band-edge positions of these two alignments, compared with the redox potential of water at  $pH = 7$ , are shown in the shaded regions of Figs. 5(a)–5(d). It can be seen that the band-edge positions of both alignments meet the requirements for photocatalytic water splitting, indicating that the CdSeTe monolayer is a promising candidate for this application. It should be noted that due to the polarization between the conduction-band valleys of the CdSeTe monolayer, the photogenerated electrons are unevenly distributed in them. The valley contributed by Te atoms has a lower energy, resulting in a higher proportion of photogenerated electrons. In contrast, the valley contributed by Se atoms has a higher energy, leading to a lower proportion of photogenerated electrons. Consequently, the photogenerated electrons from these valleys play different roles in the HER. Despite both band-edge alignments coexist in the CdSeTe monolayer, Alignment 1 is dominant.

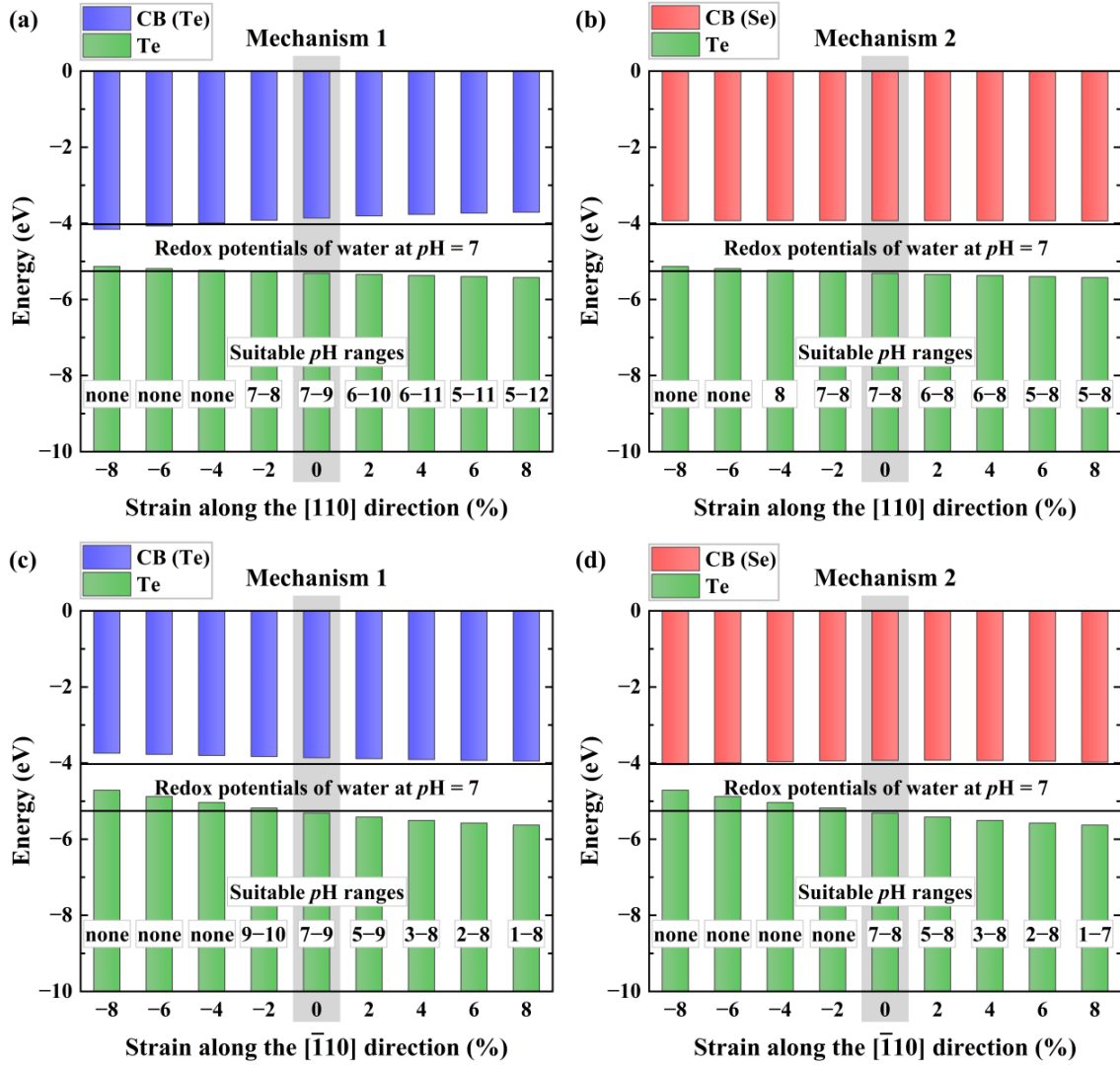


**FIG. 5** (Color online) The absolute band-edge positions of the band-edge alignments under different strains along  $[110]$  (a, b) and  $[\bar{1}\bar{1}0]$  (c, d) directions, compared to the redox potential of water at  $pH = 7$ . The gray shaded regions represent the unstrained condition. The redox potential of water is closely related to the  $pH$  of the environment, which can be described by:  $E_{H^+/H_2}^{\text{red}} = -4.44 \text{ eV} + pH \times 0.059 \text{ eV}$ ,  $E_{H_2O/O_2}^{\text{oxd}} = -5.67 \text{ eV} + pH \times 0.059 \text{ eV}$ . The annotations indicate the suitable  $pH$  ranges for photocatalytic water splitting under various strain conditions.

Finally, we apply uniaxial in-plane strains ranging from -8% to 8% along the

crystallographic directions  $[110]$  and  $[\bar{1}10]$  of the ternary pentagonal CdSeTe monolayer to modulate the polarization of valleys, accounting for the Poisson effect throughout the process. Figs. 6(a) and 6(b) present the bandgaps and the polarizations between conduction-band valleys ( $\Delta E_c$ ) under various strain conditions at the HSE06 level, where  $\Delta E_c$  is given by:  $\Delta E_c = E_{CB(Se)}^{DFT} - E_{CB(Te)}^{DFT}$ . A positive  $\Delta E_c$  indicates a lower energy in the valley contributed by Te atoms, while a negative  $\Delta E_c$  signifies a reversed polarization with a lower energy in the valley contributed by Se atoms. Applying tensile strains along the  $[110]$  direction or compressive strains along the  $[\bar{1}10]$  direction results in a decrease in  $\Delta E_c$ . Conversely, applying opposite strains leads to an increase in  $\Delta E_c$ . By varying the applied strains, we identified two critical conditions where  $\Delta E_c$  becomes zero, namely 8% tensile strain along the  $[110]$  direction and -6% compressive strain along the  $[\bar{1}10]$  direction.

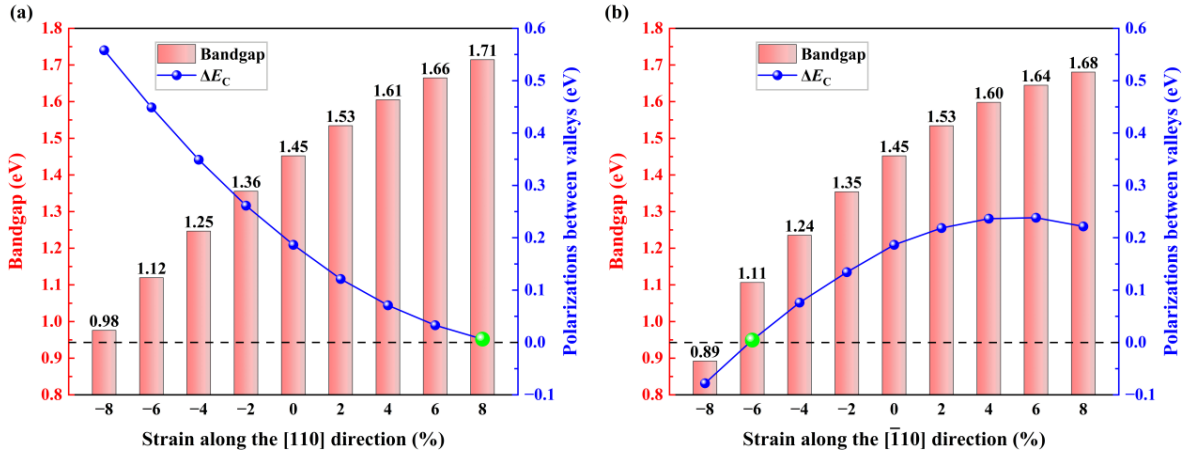


**FIG. 6** (Color online) The bandgaps and the polarizations between conduction-band valleys ( $\Delta E_c$ ) under various strain conditions along  $[110]$  (a) and  $[\bar{1}10]$  (b) directions at the HSE06 level. The left axes represent the bandgap values, while the right axes indicate the  $\Delta E_c$  values. The green data points mark the critical conditions where  $\Delta E_c$  becomes zero.

Strain alters the polarization between conduction-band valleys in the CdSeTe monolayer, which in turn affects the dominance relationship between its band-edge alignments. When the absolute value of  $\Delta E_c$  is large, it can be approximated that only one type of alignment is active, similar to the behavior observed in many 2D materials with intrinsic electric fields [45-48,68]. Conversely, when the absolute value of  $\Delta E_c$  is small, both alignments are active, but they exhibit different levels of dominance. Specifically, when the value of  $\Delta E_c$  is positive, Alignment 1 is dominant; when the value of  $\Delta E_c$  is zero, both alignments are equally significant; and when the value of  $\Delta E_c$  is negative, Alignment 2 becomes dominant. The band-edge positions of both alignments in the CdSeTe monolayer under different strains, compared with the redox potential of water at  $pH = 7$ , are shown in Figs. 5(a)–5(d). The results indicate that when tensile strain ranging from -2% to 8% along the [110] direction is applied, or compressive strain ranging from 0% to 8% along the  $[\bar{1}\bar{1}0]$  direction is applied, both alignments are active, allowing the HER to occur on both surfaces of the CdSeTe monolayer. When a -2% compressive strain along the  $[\bar{1}\bar{1}0]$  direction is applied, only Alignment 1 is active, and the HER can occur solely on the lower surface of the CdSeTe monolayer. When a -4% tensile strain along the [110] direction is applied, only Alignment 2 is active, and the HER can occur solely on the upper surface of the CdSeTe monolayer. Under other conditions, both alignments are inactive, and photocatalytic water splitting ceases. Accordingly, selective switching between the band-edge alignments can be achieved through strain engineering, allowing precise control over

which surface of the material supports the HER. This capability provides a method to control whether the products are mixed or separated, holding potential for future applications.

In summary, we have proposed a novel concept of atom-valley locking for the ternary pentagonal CdSeTe monolayer, where the spatial distribution of valleys is atom-dependent. In the CdSeTe monolayer, two valleys in the conduction band can be identified in the electronic band structure, one contributed by Se atoms on the upper surface and the other by Te atoms on the lower surface, with a spontaneous polarization of 187 meV between them. This phenomenon can be attributed to the localization of the valley electrons and the breaking of the  $S_4$  symmetry. Owing to this unique spatial distribution of valleys, two types of band-edge alignments can coexist in the CdSeTe monolayer with an intrinsic electric field. Furthermore, applying uniaxial in-plane strains can modulate the polarization of valleys, thereby altering the dominance relationship between these alignments. As a result, selective switching between them becomes possible, allowing precise control over which surface of the material supports the HER. Our findings suggest that valley manipulation holds great potential in photocatalytic applications. The possibilities for achieving valley polarization are significantly expanded by eliminating the requirement to break the time-reversal symmetry. Future exploration may lead to the discovery of new valley phenomena, novel valley manipulation techniques, and innovative applications.

## **Acknowledgments**

This work was supported by the National Natural Science Foundation of China (Grant No. 12074274) and the Natural Science Foundation of Chongqing City (Grant No. cstc2020jcyjmsxmX0616).

### **Conflict of interest**

There are no conflicts of interest to declare.

### **Data availability**

The data that support the findings of this study are available from the corresponding author upon reasonable request.

### **References**

- [1] O. Gunawan, Y. P. Shkolnikov, K. Vakili, T. Gokmen, E. P. De Poortere, and M. Shayegan, [Phys. Rev. Lett. \*\*97\*\*, 186404 \(2006\)](#).
- [2] A. Rycerz, J. Tworzydło, and C. W. J. Beenakker, [Nat. Phys. \*\*3\*\*, 172 \(2007\)](#).
- [3] D. Xiao, W. Yao, and Q. Niu, [Phys. Rev. Lett. \*\*99\*\*, 236809 \(2007\)](#).
- [4] Z. Zhu, A. Collaudin, B. Fauqué, W. Kang, and K. Behnia, [Nat. Phys. \*\*8\*\*, 89 \(2011\)](#).
- [5] D. Xiao, G.-B. Liu, W. Feng, X. Xu, and W. Yao, [Phys. Rev. Lett. \*\*108\*\*, 196802 \(2012\)](#).
- [6] H.-Z. Lu, W. Yao, D. Xiao, and S.-Q. Shen, [Phys. Rev. Lett. \*\*110\*\*, 016806 \(2013\)](#).
- [7] B. Zhu, H. Zeng, J. Dai, and X. Cui, [Adv. Mater. \*\*26\*\*, 5504 \(2014\)](#).
- [8] H. Yuan, X. Wang, B. Lian, H. Zhang, X. Fang, B. Shen, G. Xu, Y. Xu, S.-C. Zhang, H. Y. Hwang, and Y. Cui, [Nat. Nanotechnol. \*\*9\*\*, 851 \(2014\)](#).

- [9] C. Jiang, F. Liu, J. Cuadra, Z. Huang, K. Li, A. Rasmita, A. Srivastava, Z. Liu, and W.-B. Gao, [Nat. Commun. \*\*8\*\*, 802 \(2017\)](#).
- [10] R. Pisoni, A. Kormányos, M. Brooks, Z. Lei, P. Back, M. Eich, H. Overweg, Y. Lee, P. Rickhaus, K. Watanabe, T. Taniguchi, A. Imamoglu, G. Burkard, T. Ihn, and K. Ensslin, [Phys. Rev. Lett. \*\*121\*\*, 247701 \(2018\)](#).
- [11] H.-Y. Ma, M. Hu, N. Li, J. Liu, W. Yao, J.-F. Jia, and J. Liu, [Nat. Commun. \*\*12\*\*, 2846 \(2021\)](#).
- [12] L. Banszerus, S. Möller, C. Steiner, E. Icking, S. Trellenkamp, F. Lentz, K. Watanabe, T. Taniguchi, C. Volk, and C. Stampfer, [Nat. Commun. \*\*12\*\*, 5250 \(2021\)](#).
- [13] Z. Gong, G.-B. Liu, H. Yu, D. Xiao, X. Cui, X. Xu, and W. Yao, [Nat. Commun. \*\*4\*\*, 2053 \(2013\)](#).
- [14] Z.-M. Yu, S. Guan, X.-L. Sheng, W. Gao, and S. A. Yang, [Phys. Rev. Lett. \*\*124\*\*, 037701 \(2020\)](#).
- [15] X. Zhang, J. Zhou, S.-Q. Li, Y. Wang, S. Zhang, Y. Liu, J. Gao, J. Zhao, W. Wang, R. Yu, W. Zhang, N. Liu, J. Nie, L. He, and R. Dou, [J. Phys. Chem. Lett. \*\*12\*\*, 5879 \(2021\)](#).
- [16] X. Xu, Z. He, Y. Dai, B. Huang, L. Kou, and Y. Ma, [Appl. Phys. Lett. \*\*119\*\*, 073101 \(2021\)](#).
- [17] L. Jiang, C. H. Yang, Z. Pan, A. Rossi, A. S. Dzurak, and D. Culcer, [Phys. Rev. B \*\*88\*\*, 085311 \(2013\)](#).
- [18] M. V. Klymenko, S. Rogge, and F. Remele, [Phys. Rev. B \*\*95\*\*, 205301 \(2017\)](#).
- [19] B. Tariq and X. Hu, [Phys. Rev. B \*\*100\*\*, 125309 \(2019\)](#).
- [20] W.-Y. Tong, S.-J. Gong, X. Wan, and C.-G. Duan, [Nat. Commun. \*\*7\*\*, 13612 \(2016\)](#).
- [21] E. Barré, J. A. C. Incorvia, S. H. Kim, C. J. McClellan, E. Pop, H.-S. P. Wong, and T. F. Heinz, [Nano Lett. \*\*19\*\*, 770 \(2019\)](#).
- [22] H. Zeng, J. Dai, W. Yao, D. Xiao, and X. Cui, [Nat. Nanotechnol. \*\*7\*\*, 490 \(2012\)](#).
- [23] K. F. Mak, K. He, J. Shan, and T. F. Heinz, [Nat. Nanotechnol. \*\*7\*\*, 494 \(2012\)](#).

- [24] T. Cao, G. Wang, W. Han, H. Ye, C. Zhu, J. Shi, Q. Niu, P. Tan, E. Wang, B. Liu, and J. Feng, [Nat. Commun. 3, 1882 \(2012\)](#).
- [25] W.-T. Hsu, Y.-L. Chen, C.-H. Chen, P.-S. Liu, T.-H. Hou, L.-J. Li, and W.-H. Chang, [Nat. Commun. 6, 8963 \(2015\)](#).
- [26] K. F. Mak, D. Xiao, and J. Shan, [Nat. Photonics 12, 451 \(2018\)](#).
- [27] X. Xu, W. Yao, D. Xiao, and T. F. Heinz, [Nat. Physics 10, 343 \(2014\)](#).
- [28] J. Xin, Y. Tang, Y. Liu, X. Zhao, H. Pan, and T. Zhu, [npj Quantum Mater. 3, 9 \(2018\)](#).
- [29] S. A. Vitale, D. Nezich, J. O. Varghese, P. Kim, N. Gedik, P. Jarillo-Herrero, D. Xiao, and M. Rothschild, [Small 14, 1801483 \(2018\)](#).
- [30] A. Sharan and N. Singh, [Adv. Theory Simul. 5, 2100476 \(2022\)](#).
- [31] T. Zhang, S. Zhao, A. Wang, Z. Xiong, Y. Liu, M. Xi, S. Li, H. Lei, Z. V. Han, and F. Wang, [Adv. Funct. Mater. 32, 2204779 \(2022\)](#).
- [32] P. San-Jose, E. Prada, E. McCann, and H. Schomerus, [Phys. Rev. Lett. 102, 247204 \(2009\)](#).
- [33] D. Gunlycke and C. T. White, [Phys. Rev. Lett. 106, 136806 \(2011\)](#).
- [34] Y. Jiang, T. Low, K. Chang, M. I. Katsnelson, and F. Guinea, [Phys. Rev. Lett. 110, 046601 \(2013\)](#).
- [35] M. M. Grujić, M. Ž. Tadić, and F. M. Peeters, [Phys. Rev. Lett. 113, 046601 \(2014\)](#).
- [36] L. Ju, Z. Shi, N. Nair, Y. Lv, C. Jin, J. V. Jr, C. Ojeda-Aristizabal, H. A. Bechtel, M. C. Martin, A. Zettl, J. Analytis, and F. Wang, [Nature \(London\) 520, 650 \(2015\)](#).
- [37] M. Sui, G. Chen, L. Ma, W.-Y. Shan, D. Tian, K. Watanabe, T. Taniguchi, X. Jin, W. Yao, D. Xiao, and Y. Zhang, [Nat. Phys. 11, 1027 \(2015\)](#).
- [38] J. R. Schaibley, H. Yu, G. Clark, P. Rivera, J. S. Ross, K. L. Seyler, W. Yao, and X. Xu, [Nat.](#)

[Rev. Mater. \*\*1\*\*, 16055 \(2016\).](#)

[39] V. H. Nguyen, S. Dechamps, P. Dollfus, and J.-C. Charlier, [Phys. Rev. Lett. \*\*117\*\*, 247702 \(2016\).](#)

[40] M. Settnes, S. R. Power, M. Brandbyge, and A.-P. Jauho, [Phys. Rev. Lett. \*\*117\*\*, 276801 \(2016\).](#)

[41] J. Li, R.-X. Zhang, Z. Yin, J. Zhang, K. Watanabe, T. Taniguchi, C. Liu, and J. Zhu, [Science \*\*362\*\*, 1149 \(2018\).](#)

[42] A. Fujishima and K. Honda, [Nature \(London\) \*\*238\*\*, 37 \(1972\).](#)

[43] C.-F. Fu, X. Wu, and J. Yang, [Adv. Mater. \*\*30\*\*, 1802106 \(2018\).](#)

[44] X. Li, Z. Li, and J. Yang, [Phys. Rev. Lett. \*\*112\*\*, 018301 \(2014\).](#)

[45] C.-F. Fu, J. Sun, Q. Luo, X. Li, W. Hu, and J. Yang, [Nano Lett. \*\*18\*\*, 6312 \(2018\).](#)

[46] C. Xia, W. Xiong, J. Du, T. Wang, Y. Peng, and J. Li, [Phys. Rev. B \*\*98\*\*, 165424 \(2018\).](#)

[47] Y. Fan, X. Song, S. Qi, X. Ma, and M. Zhao, [J. Mater. Chem. A \*\*7\*\*, 26123 \(2019\).](#)

[48] P. Wang, H. Liu, Y. Zong, H. Wen, J.-B. Xia, and H.-B. Wu, [ACS Appl. Mater. Interfaces \*\*13\*\*, 34178 \(2021\).](#)

[49] N.-H. Qiao, C.-L. Yang, M.-S. Wang, and X.-G. Ma, [Surf. Interfaces \*\*31\*\*, 102011 \(2022\).](#)

[50] Q. Yang, D. Wang, Z.-Y. Zeng, H.-Y. Geng, and X.-R. Chen, [Phys. Rev. B \*\*109\*\*, 035411 \(2024\).](#)

[51] X. Ma, X. Wu, H. Wang, and Y. Wang, [J. Mater. Chem. A \*\*6\*\*, 2295 \(2018\).](#)

[52] R. Peng, Y. Ma, B. Huang, and Y. Dai, [J. Mater. Chem. A \*\*7\*\*, 603 \(2019\).](#)

[53] X. Lv, L. Yu, F. Li, J. Gong, Y. He, and Z. Chen, [J. Mater. Chem. A \*\*9\*\*, 6993 \(2021\).](#)

[54] Y.-Q. Li, D.-S. Tang, Q.-W. He, X. Shang, and X.-C. Wang, [Appl. Phys. Lett. \*\*122\*\*, 193903 \(2023\).](#)

[55] Y. Qi, J. Zhao, and H. Zeng, [Phys. Rev. B \*\*110\*\*, 014442 \(2024\).](#)

[56] R.-W. Zhang, C. Cui, R. Li, J. Duan, L. Li, Z.-M. Yu, and Y. Yao, [Phys. Rev. Lett. \*\*133\*\*, 056401](#)

(2024).

[57] G. Kresse, J. Furthmüller, and J. Hafner, *Europhys. Lett.* **32**, 729 (1995).

[58] G. Kresse and J. Furthmüller, *Phys. Rev. B* **54**, 11169 (1996).

[59] J. P. Perdew, K. Burke, and M. Ernzerhof, *Phys. Rev. Lett.* **77**, 3865 (1996).

[60] E. Caldeweyher, J.-M. Mewes, S. Ehlert, and S. Grimme, *Phys. Chem. Chem. Phys.* **22**, 8499

(2020).

[61] V. Wang, G. Tang, Y.-C. Liu, R.-T. Wang, H. Mizuseki, Y. Kawazoe, J. Nara, and W. T. Geng, *J. Phys. Chem. Lett.* **13**, 11581 (2022).

[62] J. Heyd, G. E. Scuseria, and M. Ernzerhof, *J. Chem. Phys.* **118**, 8207 (2003).

[63] Y. Shen and Q. Wang, *Phys. Rep.* **964**, 1 (2022).

[64] X. Liu, X. Shao, Y. Zheng, S. Qi, M. Zhang, H. Li, C. Li, M. Tan, D. Zheng, and M. Zhao, *Appl. Surf. Sci.* **518**, 146197 (2020).

[65] D. L. Duong, S. J. Yun, and Y. H. Lee, *ACS Nano* **11**, 11803 (2017).

[66] D. Zhai, C. Chen, C. Xiao, and W. Yao, *Nat. Commun.* **14**, 1961 (2023).

[67] H.-Y. Liu, C.-L. Yang, M.-S. Wang, and X.-G. Ma, *Appl. Surf. Sci.* **501**, 144263 (2020).

[68] L. Ju, M. Bie, X. Tang, J. Shang, and L. Kou, *ACS Appl. Mater. Interfaces* **12**, 29335 (2020).